Am J Transl Res 2020;12(3):743-757
www.ajtr.org /ISSN:1943-8141/AJTR0099912

Original Article

Treatment with soluble bone morphogenetic protein type 1A receptor fusion protein alleviates irradiation-induced bone loss in mice through increased bone formation and reduced bone resorption

Shen Wang[1], Jie Li[2], Huabei Sun[3], Liangwei Sha[3], Yilong Guo[3], Guanqiu Gu[3], Jiling Mao[3], Xinfa Nie[3], Ying Zhai[3], Dehong Yu[3], Juan Zhai[3], Hongnian Li[3], Xin Shan[3], Chengbai Dai[3], Xiangzhi Wu[3], Xiaobo He[4], Li Xin[5], Jun Liu[6], Ke Heng[7], Qinghe Geng[3]

[1]Department of Acupuncture, Guangxi Medical University, Nanning 530000, China; [2]Department of Orthopedics, Xuzhou Central Hospital, Southeast University, Xuzhou 221006, China; [3]Lab of Bone and Mineral Research, The Affiliated Pizhou Hospital of Xuzhou Medical University, Xuzhou 221300, China; [4]Department of Orthopedics, Yangzhou Jiangdu TCM Hospital, Yangzhou 225200, China; [5]Department of Osteoporosis, The Affiliated Hospital of Xuzhou Medical University, Xuzhou 221004, China; [6]Department of Orthopedics, The Second Affiliated Hospital of Nanjing Medical University, Nanjing 210011, China; [7]Department of Orthopedics, The Affiliated Changzhou No. 2 People's Hospital of Nanjing Medical University, Changzhou 213003, China

Received July 21, 2019; Accepted December 23, 2019; Epub March 15, 2020; Published March 30, 2020

Abstract: An increased fracture risk is often observed in cancer patients undergoing radiotherapy (RT), particularly at sites within the field of radiation. Therefore, the development of appropriate therapeutic options to prevent RT-induced bone loss is urgently needed. A soluble form of the BMP receptor type 1A fusion protein (mBMPR1A-mFc) serves as an antagonist to endogenous BMPR1A. Previous studies have shown that mBMPR1A-mFc treatment increases bone mass in both ovary-intact and ovariectomized via promoting osteoblastic bone formation and inhibiting osteoclastic bone resorption. The present study was designed to investigate whether mBMPR1A-mFc administration prevents radiation-induced bone deterioration in mice. We constructed an animal model of radiation-induced osteoporosis by exposure to a 2-Gy dose of X-rays. Micro-CT, histomorphometric, bone-turnover, and mechanical analyses showed that mBMPR1A-mFc administration prevented trabecular microarchitecture deterioration after RT because of a marked increase in bone formation and a decrease in bone resorption. Mechanistic studies indicated that mBMPR1A-mFc administration promoted osteoblastogenesis by activating Wnt/Lrp5/β-catenin signaling while decreasing osteoclastogenesis by inhibiting the RANKL/RANK/OPG pathway. Our novel findings provide solid evidence for the application of mBMPR1A-mFc as a therapeutic treatment for radiation-induced osteoporosis.

Keywords: Murine BMP receptor type 1A fusion protein (mBMPR1A-mFc), irradiation-induced osteoporosis, Wnt/Lrp5/β-catenin, RANK/RANKL/OPG

Introduction

Ionizing radiation has been used for nearly a century in cancer patients, alone or in combination with chemotherapy [1, 2], and has been proven to be an effective and indispensable treatment modality [2]. Specifically, ionizing radiation damages tumor DNA and induces tumor cell death. The efficacy of radiotherapy (RT), however, comes at the expense of normal tissue injury [3-5]. *In vitro and in vivo* findings have demonstrated that radiation reduces osteoblast proliferation and differentiation, induces cell cycle arrest, decreases collagen production, damages or kills osteoblasts, and inhibits bone formation [6, 7]. The loss of bone density, as well as the increased risk of fracture, remains a problematic side effect of RT [8-10].

The area selected for RT often includes the whole tumor and the healthy neighboring tissue. Previous work has demonstrated that a typical treatment regimen of RT for gynecologi-

cal cancers consists of an administration of up to 60 Gy fractionated over a 6-week treatment span [4, 11]. Healthy neighboring tissue, including bone, absorbs approximately 30 Gy [4, 12]. Various strategies have been developed to attenuate the deleterious effect of RT on the nearby tissues, such as precise treatment planning and delivery [13]. Despite these measures, the incidence of pathological fracture in the area selected for RT remains frequent and increases with time in cancer survivors [8, 9, 14-18]. Previous clinical studies have reported that hip fracture rates are up to 20 times higher in breast cancer patients who received RT compared to those of patients without RT [19, 20]. Patients receiving RT for pelvic tumors have an increased risk of hip fracture compared with that of tumor patients undergoing chemotherapy or surgery alone [8, 9, 15-18]. Additionally, a dose-dependent relationship between rib fracture incidence and RT has been observed in breast tumor patients [14].

Anti-resorptive drugs, such as zoledronic acid and risedronate, are clinically used to treat this deleterious effect [21, 22]. Despite their effectiveness, most of these agents have some limitations and side effects, including thromboembolism and esophageal irritation [23]. Therefore, searching for new agents to prevent or treat RT-induced bone loss is of crucial importance.

Bone morphogenetic proteins (BMPs) are an important member of the transforming growth factor-β (TGF-β) gene superfamily. BMPs control cell growth, differentiation, and function [24] and play a key role in regulating physiological functions. BMPs also act as major regulators of bone homeostasis [25]. BMP signaling is mediated by the activation of type-I and type-II receptors. Upon ligand binding, a conserved glycine- and serine-rich domain between the transmembrane and kinase domains in the type-I receptor is phosphorylated and activated. Among the three type-I receptors that recognize BMPs (BMPR1A or ALK3, BMPR1B or ALK6, and ACVRI or ALK2), BMPR1A (or ALK3) is the most effective receptor for transducing canonical BMP ligands BMP2 [26] and BMP4 [27], which is highly expressed in the bone [28].

Previous studies have reported that mice with a postnatal conditional deletion of BMPR1A experience a significant increase in bone mass [29, 30], which is associated with a reduction of the Wnt antagonists, sclerostin (SOST) and dickkopf-1 (Dkk1) [31], as well as a decrease in the receptor activator of the NF-kB ligand (RANKL) and an increase in osteoprotegerin (OPG) expression [29-34]. Additionally, a postnatal conditional BMPR1A deletion in osteoclasts causes an obviously increased bone mass [33]. All these *in vivo* results strongly suggest that inhibition of BMPR1A signaling provides therapeutic benefits for the treatment of osteoporosis.

A soluble murine BMPR1A-fusion protein (mBMPR1A-mFc) acts as an antagonist to endogenous BMPR1A, consisting of the extracellular domain of murine BMPR1A and the Fc portion of murine IgG2a. A previous study showed that mBMPR1A-mFc binds to BMP2/4 specifically and with high affinity [25], which in turn reduces Dkk1 expression in osteoblasts, activates Wnt signaling, and promotes osteoblastic bone formation [35]. Furthermore, mBMPR1A-mFc treatment markedly decreased RANKL expression in osteoblasts and inhibited bone resorption. Interestingly, treatment of ovary-intact and ovariectomized mice with mBMPR1A-mFc results in improved bone microarchitecture and strength, as well as increased bone mass, via promoting bone formation and inhibiting bone resorption [25]. These findings suggest that inhibition of BMPR1A signaling with mBMPR1A-mFc may have a positive therapeutic benefit for the treatment of pathological bone loss. Little is known, however, about its therapeutic effects on radiation-induced osteoporosis.

In this study, a focal radiation mouse model was used to evaluate the role of mBMPR1A-mFc in radiation-induced osteoporosis. Our data suggest that mBMPR1A-mFc may represent a novel therapeutic agent to treat radiation-induced osteoporosis.

Material and methods

Animals, radiation therapy, and drug administration

The Institutional Animal Care and Use Committee of Xuzhou Medical University approved all study procedures. Fifteen-week-old female C57BL/6j mice were purchased from the Experimental Animal Center of Nanjing Medical

University (Nanjing, China) and allowed to acclimate for 5 weeks, until the age of 20 weeks (n=30); commercial rodent diet and water were given ad libitum. At the start of the study, body masses were measured and used to randomize the mice between groups. Two groups were designated to receive irradiation (n=20 total). Under anesthesia (2% isoflurane), mice were irradiated. A small animal image-guided irradiation system (Precision X-Ray, North Branford, CT, USA) was used to precisely irradiate the mid-shaft of the left femur at a single dose of 2 Gy on day 1. This system offers integrated precision irradiation with cone-beam CT guidance and treatment planning systems with dose calculation tools based on the Monte Carlo methods. In brief, a single field of 140-kVp X-rays to a single-fraction mid-plane dose of 2 Gy at a rate of 1.36 Gy/min in the prone position (Philips Medical Systems, Bothell, WA, USA), as previously reported [21]. Radiation was delivered in a circular collimated field with a diameter of 5 mm at a rate of 0.23 Gy/s. A single 2-Gy dose was used in the present study to simulate a clinical radiotherapy setting consistent with that of previous studies on radiation-induced bone loss [36, 37]. One of the irradiated groups was selected for subcutaneous injections of mBMPR1A-mFc (4.5 mg/kg; Acceleron Pharma, Cambridge, MA, USA) twice a week starting immediately following the irradiation procedure (RT + mBMPR1A-mFc; n=10). Equivalent volumes of PBS were injected as a placebo into the remaining 2-Gy-irradiated (RT + VEH; n=10) mice. One group was exposed to a sham radiation procedure (Control, n=10). In the sham procedure, anesthetized control animals were placed inside the inactive X-ray unit for the same amount of time as the radiated mice. To assess new bone formation, calcein (20 mg/kg) was injected subcutaneously into each mouse at 7 days and 2 days before euthanization. All chemicals were purchased from Sigma-Aldrich (St. Louis, MO, USA) unless indicated otherwise.

Tissue collection

At 4 weeks following the initial radiation exposure, all animals were euthanized. Next, blood was isolated by cardiac puncture and was centrifuged at 3000 rpm for 10 min to separate the serum from the blood cells, rapidly frozen in liquid nitrogen, and stored at -80°C until use. Both the hind limbs and the vertebral column were collected for measurements. Adherent soft tissue was cleaned off, and the tibiae and femora were fixed in a PLP fixative (2% paraformaldehyde containing 0.075-M lysine and 0.01-M sodium periodate) at 4°C. The next day, the bones were placed in 70% ethanol.

Serum chemistry

The serum samples were evaluated using ELISA kits for alkaline phosphatase (ALP) (Sigma, St. Louis, MO, USA), procollagen 1 N-terminal peptide (P1NP) (Immunodiagnostic Systems, Fountain Hills, AZ, USA), C-telopeptide fragments of collagen type 1 (CTX-1) (Immunodiagnostic Systems Inc., Gaithersburg, MD, USA), and tartrate-resistant acid phosphatase 5b (TRAP5b) (Immunodiagnostic Systems, London, UK), following the protocols recommended by the manufacturers.

Dual-energy X-ray absorptiometry and micro-CT

Areal BMD (aBMD) was measured by a small animal dual-energy X-ray absorptiometer (DXA) (Lunar Corp., Madison, WI, USA). The bone architecture of the distal femur was analyzed using a high-resolution micro-CT (GE Healthcare, Madison, WI, USA) with isotropic voxels of 9 μm/side, as described previously [38]. The bone histomorphometric parameters for the distal metaphysis of the femur were measured as described in the report of the American Society of Bone and Mineral Research (ASBMR) Histomorphometry Nomenclature Committee [39]. Both trabecular and cortical bone parameters-including trabecular bone volume/total volume (BV/TV, %), connectivity density (Conn.D, 1/mm^3), trabecular number (Tb.N, 1/mm^3), trabecular thickness (Tb.Th, μm), trabecular separation (Tb.Sp, μm), and structure model index (SMI)-were determined. The cortical bone parameters, including cortical area (Ct.Ar, mm^2) and cortical thickness (Ct.Th, μm), were also quantified.

Three-point bending test

The femoral shaft (n=10, for each group) was subjected to a three-point bending test to detect the whole-bone structural properties, as described previously [40], using a standard mechanical testing device (Bose ElectroForce 3220; Bose Corp., Eden Prairie, MN, USA). The

parameters of structural properties-including maximum load (N), yield load (N), yield displacement (μm), stiffness (N/mm), energy absorption (N × mm), and ultimate displacement (μm)-were determined from the load-displacement curve.

Nanoindentation

The distal femur was mounted within the Agilent G200 nanoindentation system (Agilent Technologies Inc., Chandler, AZ, USA). The force-displacement curve was automatically recorded, and the trabecular bone elastic modulus (GPa) and contact hardness (GPa) were calculated according to a protocol described previously [40].

Bone histomorphometric studies

Static and dynamic histomorphometries were conducted as described previously [41, 42]. In brief, the femurs were decalcified in an EDTA and glycerol solution for 14 days. The decalcified femurs were dehydrated and embedded in paraffin and 5-μm sections were then cut on a rotary microtome. The sections were stained with hematoxylin and eosin (HE), total collagen, toluidine blue, von Kossa, ALP, and tartrate-resistant acid phosphatase (TRAP). The static parameters of bone formation and resorption were measured using an Olympus microscope with an OsteoMeasure system (Osteometrics). As the static parameters, Tb.BV/TV (%), total collagen positive areas/tissue area (%), von Kossa positive area/tissue area (%), number of OBs per bone surface (N.Ob/BS, N/mm), percentage of bone surfaces covered by OBs (Ob.S/BS, %), ALP-positive areas/tissue area (%), number of osteoclasts per bone surface (N.Oc/BS, N/mm), eroded bone surface (ES/BS, %), and bone surface occupied by osteoclasts (Oc.S/BS, %) were measured.

For fluorochrome-based determination of the rates of bone formation by dynamic histomorphometry, 6-μm frozen sections embedded in methyl methacrylate plastic were cut using a Leica RM2265 rotary microtome (Leica, Heidelberg, Germany). Calcein was visualized by fluorescent microscopy, and the distance between labeled layers was used as a measure of the rate of bone formation as determined by the morphometry software. Mineralizing surface per bone surface (MS/BS, %) and the mineral apposition rate (MAR, mm/day) were measured and used to calculate the bone formation rate (BFR, mm^3/mm^2/day), as described previously [42]. The terminology and units used were those recommended by the Histomorphometry Nomenclature Committee of the American Society for Bone and Mineral Research [43].

Quantitative PCR

Total RNA was isolated from tibia with Trizol reagent (Invitrogen, Carlsbad, CA, USA) according to the manufacturer's protocol. Real-time RT-PCR was performed as described previously [42, 44]. The primers used for the real-time PCR were purchased commercially. All PCRs were performed in triplicate, and the primer sequences used for PCR are shown in **Table 1**.

Western blot analysis

Proteins were isolated from the distal tibiae and were measured with a protein assay kit (Bio-Rad, Mississauga, ON, Canada). Protein samples (15 μg) were separated by SDS-PAGE and transferred to nitrocellulose membranes. Membranes were blotted with primary antibodies against β-catenin (ab16051, Abcam, Cambridge, MA, USA), and GAPDH (ab8245, Abcam, Cambridge, MA, USA) was used as the loading control. Immunoblotting was carried out as described previously [41]. Bands were visualized and quantitated by ScionImage Beta 4.02 (Scion Corporation, Frederick, MD, USA).

Statistical analysis

Data are expressed as the mean ± standard error of the mean. All statistical comparisons were conducted using one-way analysis of variance and a Newman-Keuls post-hoc test; the threshold for significance for all tests was set at a 5% probability of a type-I error (P=0.05). Statistical calculations were performed using Prism 4.0c (GraphPad Software, La Jolla, CA, USA).

Results

mBMPR1A-Fc treatment prevents radiation-induced bone mass loss

Following RT, the aBMD values of the whole body (**Figure 1D**), lumbar spine (**Figure 1C**), distal femoral metaphysis (**Figure 1A**), and proximal tibial metaphysis (**Figure 1B**) were obvi-

Table 1. The primer sequence for qRT-PCR

Gene	Primer	Primer sequence (5'-3')
ALP	F	CCTAGACACAAGCACTAACACTA
	R	GTCAGTCAGGTTGTTCCGATTC
RUNX2	F	CTGTGGTTACCGTCATGGCC
	R	GGAGCTCGGCGGAGTAGTTC
OCN	F	GCCTTCATGTCCAAGCAGGA
	R	GCGCCGGAGTCTGTTCACTA
Osterix	F	CATCTAACAGGAGGATTTTGGTTTG
	R	AAGCCTTTGCCCACCTACTTTT
Col-1A	F	CCCTACTCAGCCGTCTGTGC
	R	GGGTTCGGGCTGATGTACC
TRAP	F	CACTCCCACCCTGAGATTTGT
	R	CCCCAGAGACATGATGAAGTCA
CTSK	F	CTTCCAATACGTGCAGCAGA
	R	TCTTCAGGGCTTTCTCGTTC
NFATc1	F	GGTAACTCTGTCTTTCTAACCTTAAGCTC
	R	GTGATGACCCCAGCATGCACCAGTCACAG
ATP6vOd2	F	AAGCCTTTGACGCTGT
	R	GCCAGCACATTCATCTGTACC
Ahr	F	GGGACCTCGGGTGACAATAA
	R	CCTCTGTCCTTTTCCAACCG
Axin2	F	CAGTGTGAAGGCCAATGGC
	R	TGGGTTCTCGGAAAATGAGG
Cyr61	F	GTGAAGTGCGTCCTTGTGGA
	R	TGCCCTTTTTTAGGCTGCTG
Nkd2	F	AATTTCAGTCCAAGCACGCC
	R	CGGGACTCTCTCTCCTCTTGC
Tagln	F	CAGCCCAGACACCGAAGCTA
	R	AGGCTTGGTCGTTTGTGGAC
TGFβ-3	F	AGGCTTGGTCGTTTGTGGAC
	R	AGGCTGATTGTGGCCAAGTT
Thbs1	F	GGACCGGGCTCAACTCTACA
	R	AGCTCCGCGCTCTCCAT
Twist1	F	TCGACTTCCTGTACCAGGTCCT
	R	CCATCTTGGAGTCCAGCTCG
Wisp1	F	ATGCCTGGCTGTGTACCAGC
	R	CCTGCGAGAGTGAAGTTCGTG
TCF	F	CAGCTCCCCCATACTGTGAG
	R	TGCTGTCTATATCCGCAGGAA
Lef 1	F	CAGCTCCCCCATACTGTGAG
	R	TGCTGTCTATATCCGCAGGAA
Wnt3a	F	GGCTCCTCTCGGATACCTCT
	R	ACAGAGAATGGGCTGAGTGC
β-catenin	F	CCTAGCTGGTGGACTGCAGAA
	R	CACCACTGGCCAGAATGATGA
LRP5	F	CACCATTGATTATGCCGACCAG
	R	TGAGTCAGGCCAAACGGGTAG
RANKL	F	GCAGCATCGCTCTGTTCCTGTA
	R	CCTGCAGGAGTCAGGTAGTGTGTC
OPG	F	CACACGAACTGCAGCACATT
	R	TCCACCAAAACACTCAGCCA

ously reduced. As expected, treatment with mBMPR1A-Fc almost completely prevented the negative effects of RT on bone density (**Figure 1A-D**).

Representative mCT images of distal femur metaphysis in the three treated groups are shown in **Figure 1E**. The Ct.Th, Ct.Ar, and Ct.V values were unchanged (data not shown). RT led to a significant decrease in the trabecular microarchitecture. The BV/TV (**Figure 1F**), Conn.D (**Figure 1G**), Tb.N (**Figure 1H**), Tb.Th (**Figure 1I**), and BS/BV (**Figure 1J**) values in the RT + VEH group were significantly lower, while the Tb.Sp, (**Figure 1K**) and SMI (**Figure 1L**) values in the RT + VEH group were significantly higher than those in the control. An mBMPR-1A-Fc administration reversed these defects (**Figure 1F-L**). There was no obvious difference between the RT + mBMPR1A-Fc group and the control group, suggesting that the mBMPR1A-Fc administration completely prevented RT-induced trabecular bone loss.

mBMPR1A-Fc treatment prevents RT-induced reduction of mechanical properties

The femoral biomechanical structural properties were measured in the three-point bending test (**Figure 2A-F**). RT led to a significant decrease in biomechanical parameters, including maximum load (**Figure 2A**), yield load (**Figure 2B**), yield displacement (**Figure 2C**), stiffness (**Figure 2D**), energy absorption (**Figure 2E**), and ultimate displacement (**Figure 2F**), compared with these parameters in the control group. The femoral biomechanical material properties were examined in the nanoindentation test (**Figure 2G**, **2H**). RT resulted in obvious reductions in the tissue-level modulus (**Figure 2G**) and hardness (**Figure 2H**) as compared to these parameters in the control group. As expected, the mBMPR1A-Fc administration reversed the decrease in these biomechanical structural and material properties. No significant difference was observed between the RT + mBMPR1A-Fc group and the control group.

mBMPR1A-Fc enhances osteoblastogenesis

Representative static histomorphometric images for each group obtained by HE, total

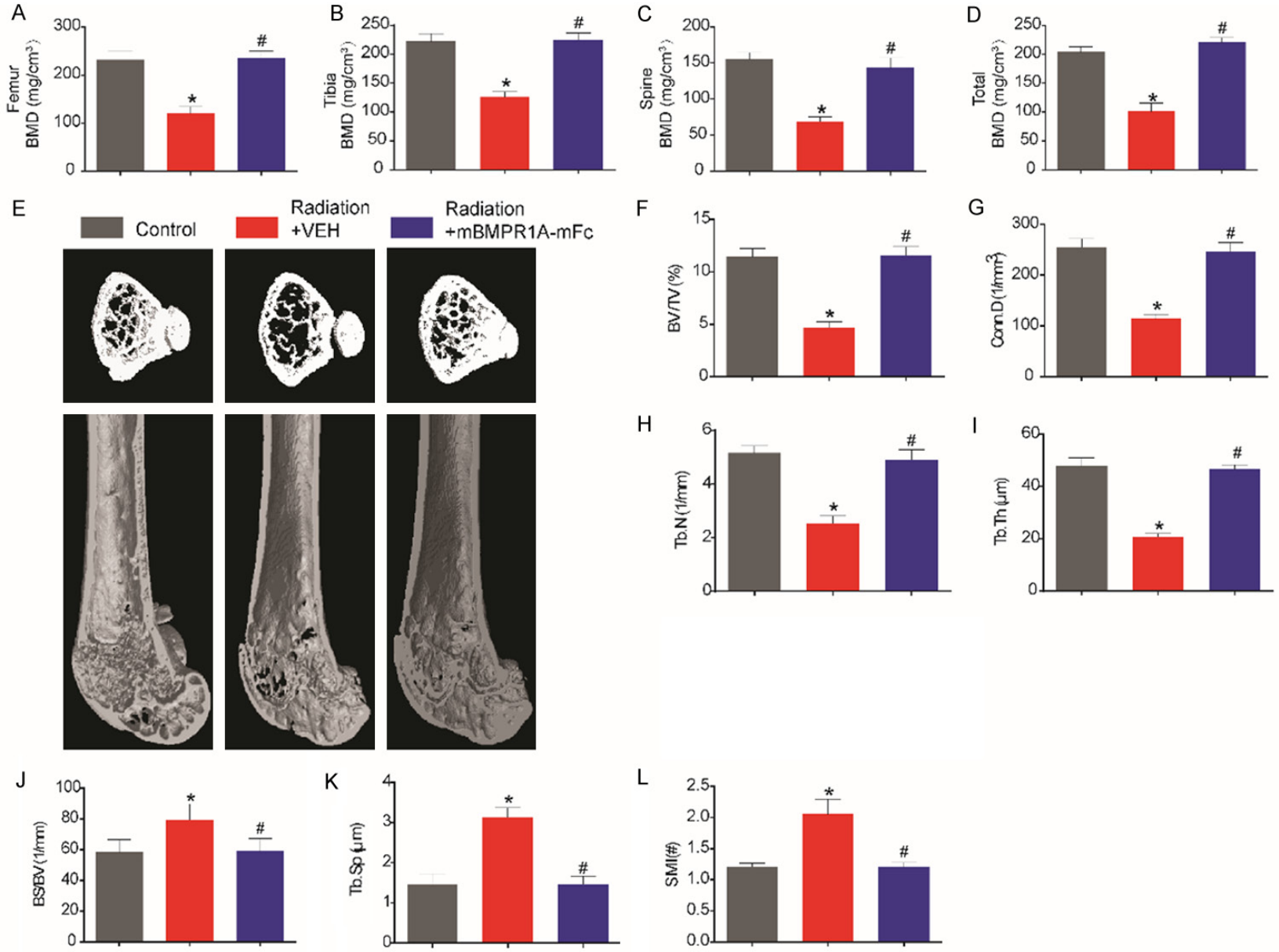
A
Femur BMD (mg/cm³)
B
Tibia BMD (mg/cm³)
C
Spine BMD (mg/cm³)
D
Total BMD (mg/cm³)
E
Control
Radiation +VEH
Radiation +mBMPR1A-mFc
F
BV/TV (%)
G
Conn.D (1/mm³)
H
Tb.N (1/mm)
I
Tb.Th (μm)
J
BS/BV (1/mm)
K
Tb.Sp (μm)
L
SMI (#)

Figure 1. mBMPR1A-mFc treatment protects against radiation-induced bone loss. (A-D) The femur, tibia, spine, and total BMD were measured by DXA. (E) Representative reconstructed μCT images of distal femurs cancellous bone and cortical bone (3D). (F) The trabecular bone volume/total volume (BV/TV), (G) connectivity density (Conn.D), (H) trabecular number (Tb.N), (I) trabecular thickness (Tb.Th), (J) bone surface to bone volume ratio (BS/BV), (K) trabecular separation (Tb.Sp), and (L) structure model index (SMI) from μCT analysis. Values are all expressed as mean ± SD, n=10 per group. *, P<0.05, versus the control group. #, P<0.05, versus the Radiation + VEH group.

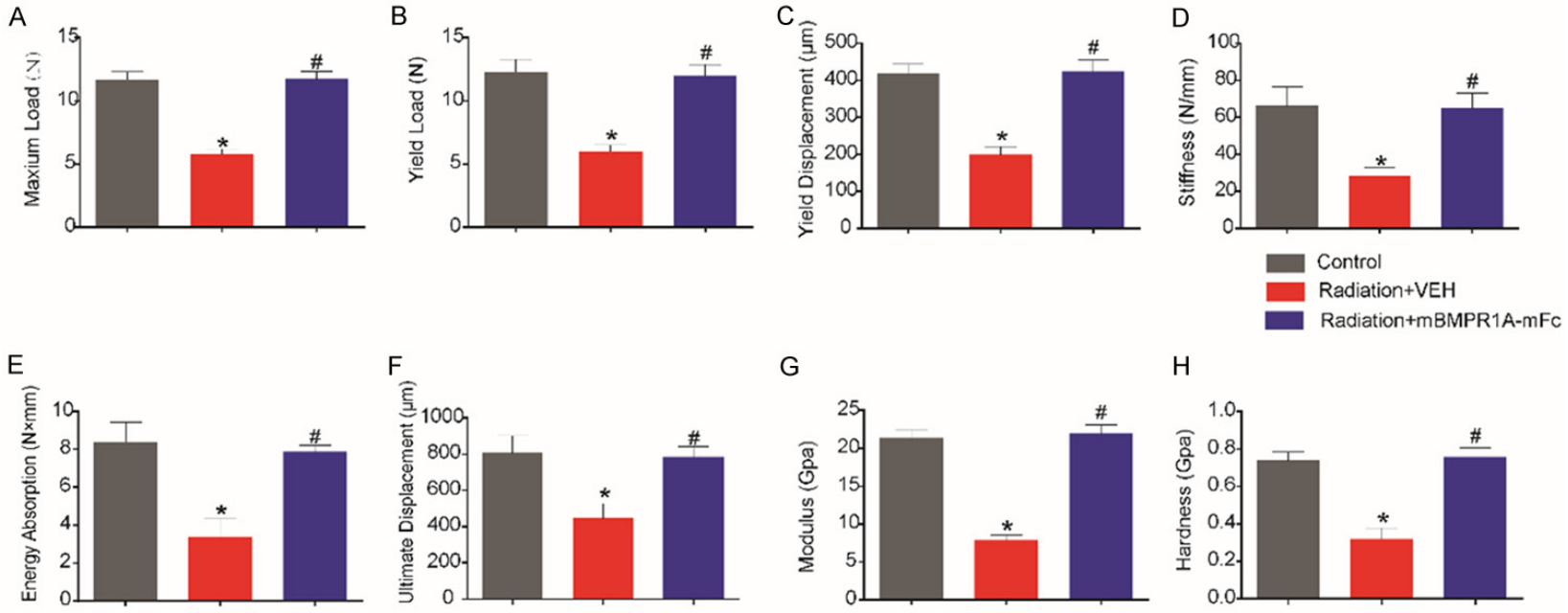

Figure 2. mBMPR1A-mFc treatment protects against radiation-induced reduction of mechanical properties. (A) The maximum load, (B) yield load, (C) yield displacement, (D) stiffness, (E) energy absorption and (F) ultimate displacement through three-point bending test. The (G) moudulus and (H) hardness through the nanoindentation system. Values are all expressed as mean ± SD, n=10 per group. *, P<0.05, versus the control group. #, P<0.05, versus the Radiation + VEH group.

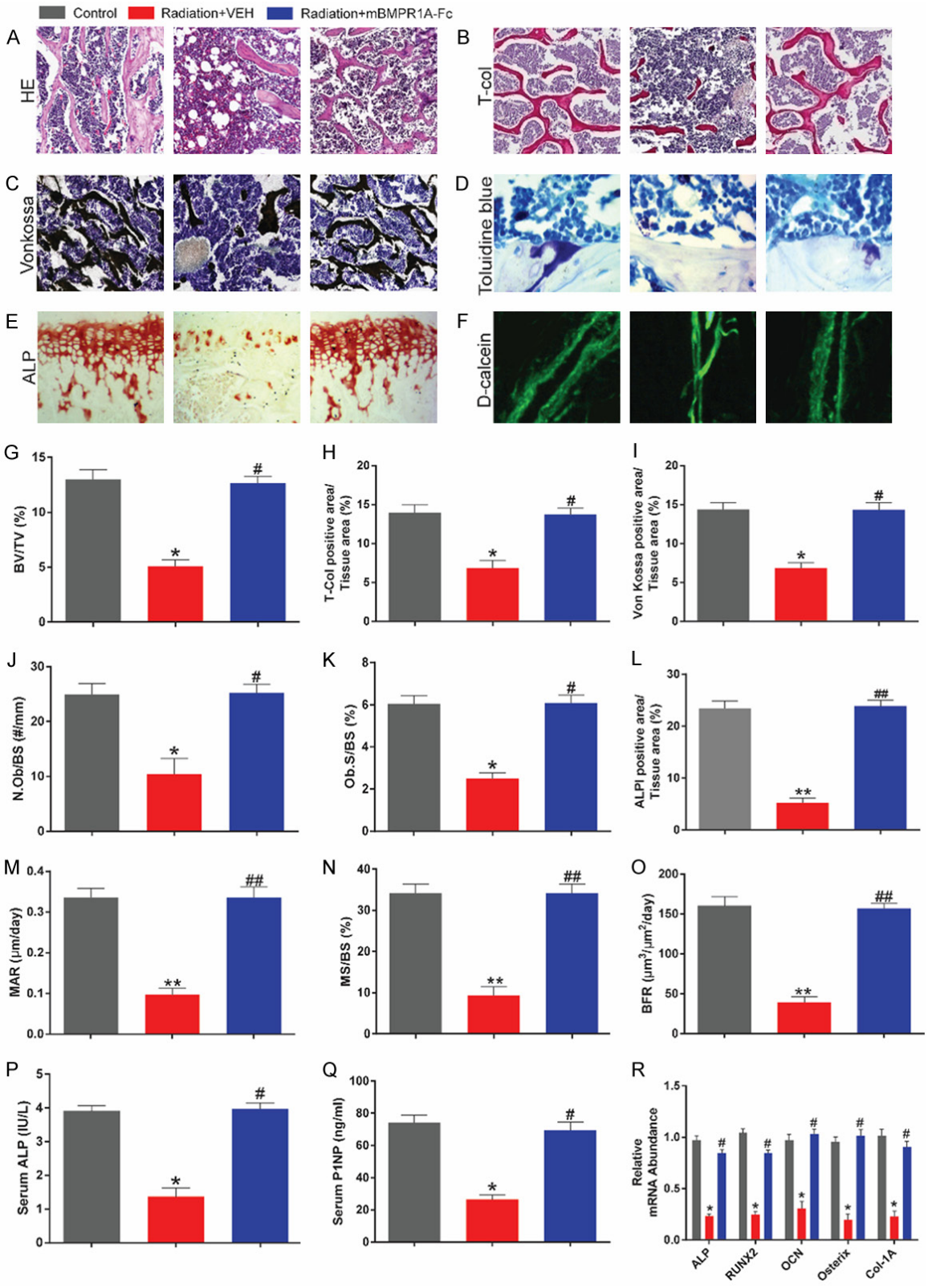

Figure 3. mBMPR1A-mFc treatment protects against the radiation-induced reduction of osteoblastic bone formation. The histomorphometric analysis of distal femur by (A) hematoxylin & eosin (H&E), 400×, (B) total collagen, 400×, (C) von kossa, 400×, (D) toluidine blue, 400×, (E) ALP, 400×, and (F) fluorescent calcein labeling staining, 400×. The histomorphometric analysis of (G) trabecular bone volume/total volume (BV/TV), (H) T-Col positive area/

Tissue area, (I) von kossa positive area/tissue area, (J) Number of OBs per bone surface (N.Ob/BS), (K) Percentage of bone surfaces covered by OBs (Ob.S/BS), (L) ALP positive area/Tissue area, (M) Mineral apposition rate (MAR), (N) Percentage of bone surfaces covered by mineralized surfaces (MS/BS) and (O) Bone formation rate/bone surface (BFR/BS). Serum bone formation markers (P) ALP, and (Q) PINP were measured by ELISA. (R) The expression of OB-specific genes, including ALP, Runx2, OCN, Osterix, and Col-1A were examined by qRT-PCR in femurs. Values are all expressed as mean ± SD, n=10 per group. *, P<0.05; **, P<0.01, versus the control group. #, P<0.05; ##, P<0.01, versus the Radiation + VEH group.

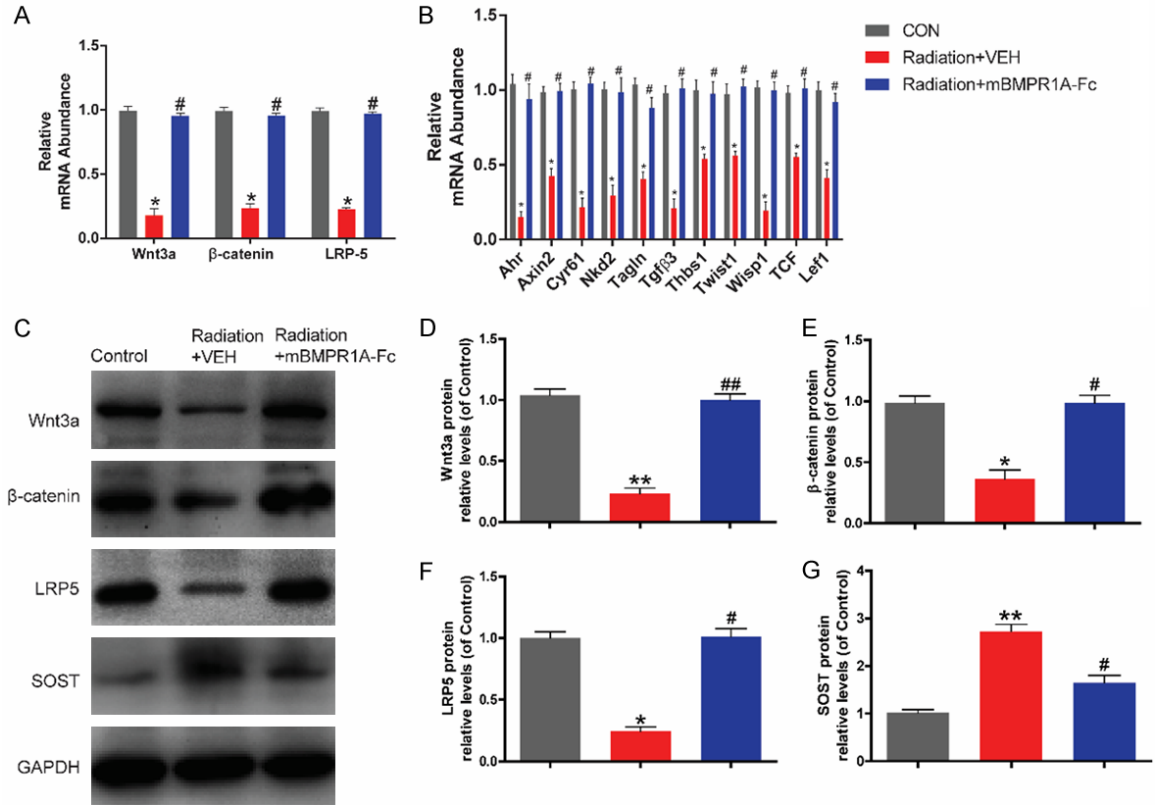

Figure 4. mBMPR1A-mFc treatment alters Wnt/β-catenin signaling. A. RT-PCR of bone tissue extracts for the expression of Wnt3a, LRP5 and β-catenin. B. RT-PCR analysis of mRNA expression of genes specifically upregulated by Wnt signaling in flushed femurs. C. Protein expression of Wnt3a, LRP5, β-catenin and SOST in each group, as assessed by Western blot analysis. D-G. Densitometry results of Wnt3a, LRP5, β-catenin and SOST protein expression in each group. Values are all expressed as mean ± SD, n=10 per group. *, P<0.05; **, P<0.01, versus the control group. #, P<0.05; ##, P<0.01, versus the Radiation + VEH group.

collagen, toluidine blue, von Kossa, and ALP staining are shown in **Figure 3A-E**. RT led to an obvious decrease in the trabecular bone in the femur compared with that of the control group, which was characterized by a significant reduction in the BV/TV (**Figure 3G**), total collagen positive areas/tissue area (**Figure 3H**), von Kossa positive area/tissue area (**Figure 3I**), ALP-positive areas/tissue area (**Figure 3L**), N.Ob/BS (**Figure 3J**), and Ob.S/BS (**Figure 3K**) compared with these parameters in the control group. Next, mBMPR1A-Fc treatment markedly attenuated the RT-induced deterioration of the femur microarchitecture. A dynamic histomorphometric (**Figure 3F**) analysis revealed that mBMPR1A-Fc administration significantly increased new bone formation at the trabecular bone, as reflected by increases in MAR (**Figure 3M**), BFR (**Figure 3N**), and MS/BS (**Figure 3O**), which, otherwise, in the absence of treatment were greatly reduced after RT (**Figure 3E**, **3M-O**). Additionally, significant decreases in serum ALP and P1NP levels were observed in the RT-VEH group compared with those of the control group. After mBMPR1A-Fc treatment, serum ALP and P1NP in the RT-mBMPR1A-Fc group were significantly higher than those in the RT-VEH group (**Figure 3P**,

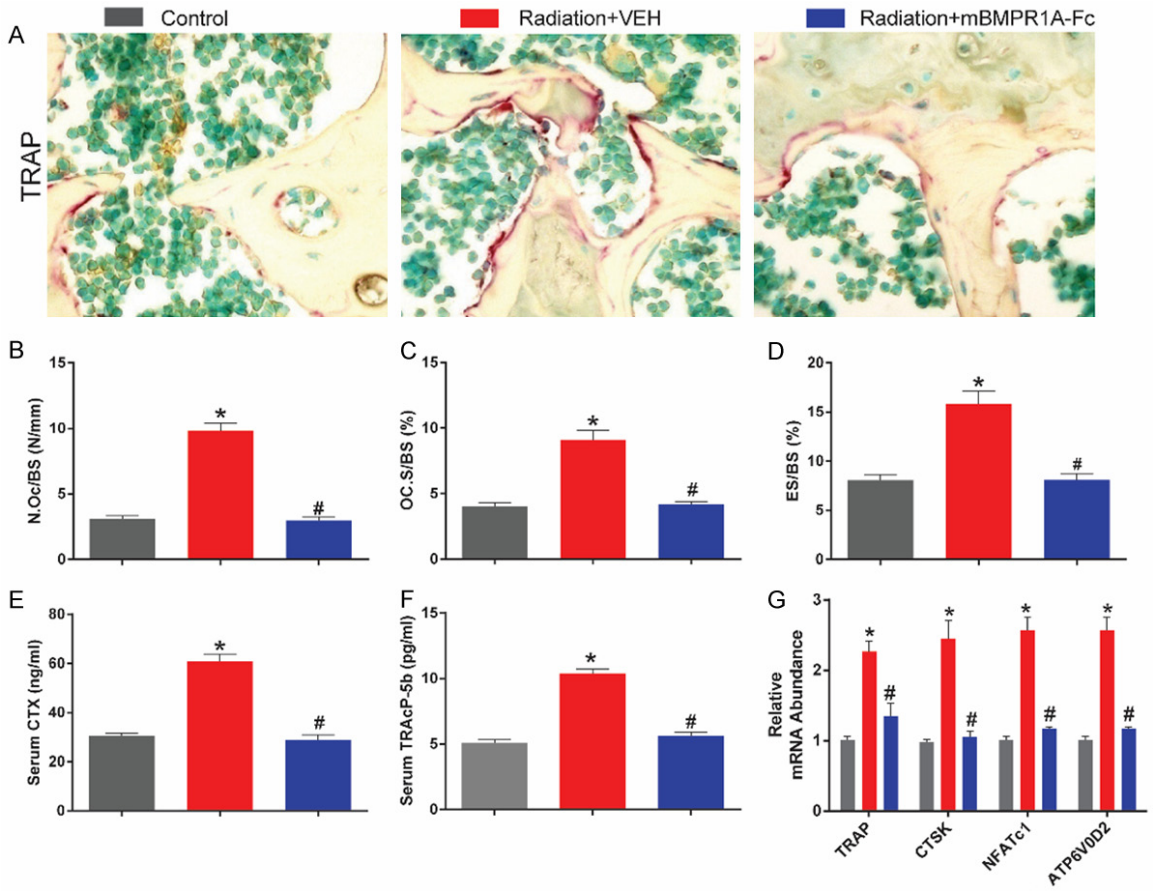

Figure 5. mBMPR1A-mFc treatment protects against the radiation-induced osteoclastic bone resorption. (A) Sections of the metaphyseal regions of the distal femurs were performed TRAP staining, 400×. (B) The osteoclast number/bone surface (N.Oc/BS), (C) Osteoclast surface/bone surface (Oc.S/BS) and (D) Eroded surface/bone surface (ES/BS) were analyzed. Serum bone resorption markers (E) CTX and (F) TRAP5b were measured by ELISA. (G) The expression of OC-specific genes, including TRAP, CTSK, NFATc1 and ATP6V0D2 were examined by qRT-PCR in femurs. Values are all expressed as mean ± SD, n=10 per group. *, P<0.05, versus the control group. #, P<0.05, versus the Radiation + VEH group.

3Q). Furthermore, the mRNA levels of ALP, Runx2, OCN, Osterix, and Col-1A were assessed by RT-PCR (**Figure 3R**). RT markedly downregulated the mRNA levels of these osteogenic genes. Expectedly, mBMPR1A-mFc administration significantly increased the expression levels of these osteogenic genes in RT mice (**Figure 3R**).

mBMPR1A-Fc promotes Wnt3a/Lrp5/β-catenin signaling pathway

Canonical Wnt3a/Lrp5/β-catenin signaling plays a crucial role in regulating the bone mass and the bone strength. In our present study, the mRNA expression levels of Wnt3a, Lrp5, and β-catenin in the three groups are listed in **Figure 4A**. These mRNA expression levels in the RT + VEH group were significantly lower than in the control group. However, the mRNA expression levels of Wnt3a, β-catenin, and Lrp5 in the RT + mBMPR1A-Fc group were significantly higher than in the RT + VEH group. In addition, we measured the mRNA expression of genes specifically upregulated by the Wnt signaling in flushed femurs. The investigated genes consisted of the following: aryl-hydrocarbon receptor (Ahr), axin2, cysteine-rich protein 61 (Cyr61), naked cuticle 2 homolog (Nkd2), transgelin (tagline), transforming growth factor β3 (TGFβ3), thrombospondin 1 (Thbs1), twist gene homolog 1 (Twist1), Wnt1-inducible signaling pathway protein 1 (Wisp1), T-cell factor (TCF), and lymphoid enhancer factor-1 (Lef-1). These genes were selected since they are sensitive markers of Wnt signaling activation [45]. The mRNA levels for the 11 studied genes were

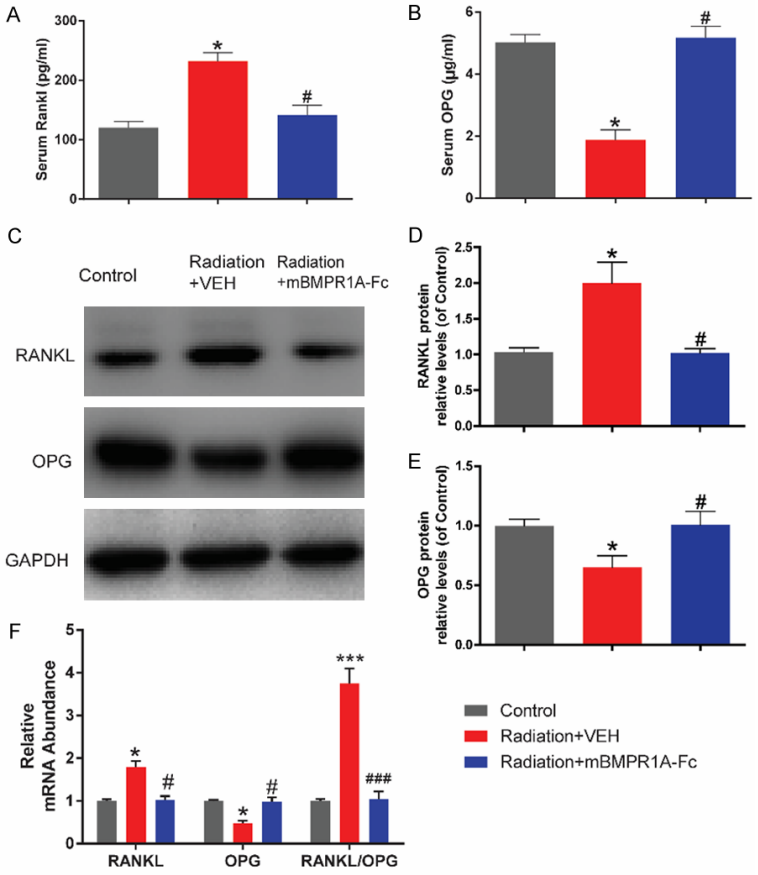

Figure 6. mBMPR1A-mFc treatment alters RANKL/OPG signaling. (A, B) Serum Rankl and OPG were measured by ELISA. Serum (A) Rankl and (B) OPG. (C) Protein expression of RANKL and OPG in each group, as assessed by Western blot analysis. (D, E) Densitometry results of RANKL and OPG protein expression in each group. (F) qPCR analysis of mRNA expression of RANKL, OPG, and RANKL/OPG ratio in femurs. Values are all expressed as mean ± SD, n=10 per group. *, P<0.05; **, P<0.01; ***, P<0.001, versus the control group. #, P<0.05; ##, P<0.01; ###, P<0.001, versus the Radiation + VEH group.

all profoundly reduced by RT compared with those of the control group. However, the mBMPR1A-Fc treatment significantly increased the mRNA expression of the 11 studied genes in mice belonging to the RT-mBMPR1A-mFc group (**Figure 4B**). Furthermore, the protein expression levels of Wnt3a, β-catenin, Lrp5 and SOST were reduced significantly in RT-VEH mice compared with that in the control mice; however, the parameters were normalized by mBMPR1A-mFc administration (**Figure 4C-G**). These results demonstrated that mBMPR1A-mFc stimulated bone formation by activating Wnt signaling.

mBMPR1A-Fc inhibits osteoclastogenesis

Representative TRAP staining (400× magnification) of femurs is shown in **Figure 5A**. A histomorphometric analysis revealed a significant increase in the N.Oc/BS (**Figure 5B**), Oc.S/BS (**Figure 5C**), and ES/BS (**Figure 5D**) in the RT-VEH group compared with that of the control mice. Consistent with the increased osteoclast numbers in the RT-VEH group, serum CTX-1 (**Figure 5E**) and TRAP-5b (**Figure 5F**) levels were also increased, reflecting increased osteoclastic bone resorption after RT. Additionally, the RT-PCR results revealed that genes related to osteoclastogenesis, such as TRAP, CTSK, NFATc1, and ATP6V0D2, were all significantly increased after RT (**Figure 5G**). Interestingly, the osteoclast numbers, bone resorption markers, and osteoclastogenic gene expressions were significantly reduced by mBMPR1A-Fc administration, to levels similar to those in the control mice (**Figure 5A-G**).

mBMPR1A-Fc inhibits RANKL/RANK/OPG signaling pathway

RANKL and OPG are cytokines predominantly secreted by osteoblasts. The relative concentration of RANKL and OPG (RANKL/OPG ratio) plays a critical role in determining bone mass and strength. RT-VEH mice exhibited a marked elevation of serum RANKL (**Figure 6A**) and a significant reduction of serum OPG as compared to those in the control (**Figure 6B**). Additionally, mBMPR1A-Fc administration reversed the adverse effects of RT on these serum markers. Consistent with the serum levels of RANKL and OPG, the protein expression and mRNA levels of OPG were significantly reduced in the RT + VEH group when compared with the control group and were associated with significant elevations in the protein expression and mRNA levels of RANKL (**Figure 6C-F**). Next, mBMPR1A-Fc administration significantly increased protein expression and mRNA levels of OPG and reduced protein expression and mRNA levels of RANKL (**Figure 6C-F**), resulting in a significant decrease in the RANKL/OPG ratio in mRNA levels.

Discussion

In spite of its efficiency in killing tumor cells, clinical RT causes secondary damage to adjacent bones. Cancer patients treated with RT develop increased fracture risks at the irradiated sites [8-10]. Thus, it is important to find appropriate treatments for RT-induced osteoporosis. In this study, we used an RT-induced osteoporosis mouse model, which revealed that impaired bone formation, as well as accelerated bone resorption, are key mechanisms mediating RT-induced osteoporosis. Furthermore, we demonstrated that mBMPR1A-mFc, an antagonist to endogenous BMPR1A, preserved the skeletal system in mice after RT. We found that mBMPR1A-mFc administration promoted bone formation and inhibited bone resorption, resulting in protection of the integrity and mechanical strength of the trabecular bone after RT. Additionally, the mBMPR1A-mFc might regulate the bone via the Wnt3a/Lrp5/β-catenin and RANKL/RANK/OPG signaling pathways.

Radiation promotes osteoclastogenesis [46]. In this study, Oc.S/BS and Oc.N/BS were obviously increased after radiation. Moreover, the mRNA levels of TRAP, Ctsk, NFATc1, and ATP6V0D2 in the femurs of the RT-VEH group were considerably higher than those of the control group. TRAP is a critical cytochemical marker enzyme that regulates the growth and differentiation of osteoclasts. As a cysteine protease secreted by osteoclasts, Ctsk is essential for the degradation of matrix collagen [47, 48]. Furthermore, NFATc1 integrates RANKL signaling during terminal differentiation of osteoclasts [49]. Additionally, ATP6V0D2 is a key molecule for osteoclast cell-cell fusion [50]. In the present study, the increases in NFATc1, Ctsk, and ATP6V0D2 mRNA levels were compatible with the histomorphometric findings and bone metabolism markers in the RT + VEH group. Consistent with a previous study [46], the current study demonstrated that the RANKL mRNA expression was upregulated, while OPG was downregulated after 4-week RT in mice. As a result, the RANKL/OPG mRNA ratio was markedly higher in the RT-VEH group than that in the control group, which is consistent with the findings of other studies [46].

Our data showed that the Oc.S/BS, Oc.N/BS, serum CTX-1, and TRACP-5b levels in the RT-mBMPR1A-mFc group were significantly lower than those in the RT-VEH group. Furthermore, mBMPR1A-mFc treatment significantly downregulated mRNA expressions of RANKL and upregulated OPG. The RANKL/OPG mRNA ratio was downregulated by mBMPR1A-mFc. Additionally, mBMPR1A-mFc administration downregulated the mRNA levels of TRAP, Ctsk, NFATc1, and ATP6V0D2 in the femur. Our results implied that RT-induced osteoclastogenesis was inhibited by mBMPR1A-mFc, which is consistent with the findings of previous studies [25, 35]. In summary, our study indicated that mBMPR1A-mFc administration regulated the RANKL/RANK/OPG signaling pathway to inhibit bone resorption, leading to improved femoral trabecular bone mass and mechanical strength in RT-treated mice.

The Wnt/Lrp5/β-catenin pathway plays a crucial role in regulating bone formation and bone resorption [51-55]. In accordance with previous studies [46], the major gene expressions in the femurs of the canonical Wnt signaling pathway, including Wnt3a, Lrp5, and β-catenin, were significantly downregulated in the RT-VEH group compared with the control group in this study. Furthermore, we analyzed the mRNA expression of genes specifically upregulated by Wnt signaling in femurs. These genes were chosen as they are sensitive markers of Wnt signaling activation [45]. The results revealed that the levels of mRNA for the 11 tested genes were all dramatically decreased by RT compared with the control group. All of these results indicated that the Wnt3a/Lrp5/β-catenin signaling was downregulated by RT, which is consistent with the findings of a previous study [56]. Interestingly, the expressions of Wnt3a, Lrp5, β-catenin, and the 11 chosen genes were all significantly upregulated after mBMPR1A-mFc administration, indicating the potential activation of the Wnt3a/Lrp5/β-catenin signaling pathway by mBMPR1A-mFc administration. Similar results have also been reported by previous studies [25]. Our study indicated that mBMPR1A-mFc upregulated the Wnt3a/Lrp5/β-catenin signaling pathway to promote bone formation, resulting in improved femur trabecular bone mass and mechanical strength in RT-induced osteoporosis mice.

A limitation of our present study was that we studied only female mice at a single time point, with a single dosing regimen for mBMPR1A-

mFc administration. Therefore, whether longer treatment at a higher dose or more frequent dosing of mBMPR1A-mFc would have greater osteoprotective effects in RT animal models remains unclear. Additional in-depth experimental work is required to determine the optimal dose and investigate the possible mechanisms responsible for the protective effects of mBMPR1A-mFc against RT-induced osteoporosis.

In conclusion, our study indicated that mBMPR1A-mFc administration could alleviate radiation-induced osteoporosis in mice, as evidenced by serum biochemical, biomechanical, micro-CT, and histological analyses. The bone-protective effects of mBMPR1A-mFc might be attributed to a combination of promoting bone formation and suppressing bone resorption. Moreover, several signaling pathways may be involved in the underlying mechanisms, including the Wnt3a/Lrp5/β-catenin and RANKL/RANK/OPG pathways. This observation suggests that mBMPR1A-mFc is a safe and effective dual-action therapeutic agent that may be effective against radiation-induced bone loss by promoting bone formation while inhibiting resorption.

Acknowledgements

This study was supported by the Research Funding Project of Xuzhou Medical University (Grant No. 2018KJ23).

Disclosure of conflict of interest

None.

Address correspondence to: Dr. Qinghe Geng, Lab of Bone and Mineral Research, The Affiliated Pizhou Hospital of Xuzhou Medical University, Xuzhou 221300, China. Tel: +86-516-8624-2323; Fax: +86-516-8260-0120; E-mail: daishan6091115@163.com; Dr. Ke Heng, Department of Orthopedics, The Affiliated Changzhou No. 2 People's Hospital of Nanjing Medical University, Changzhou 213003, China. E-mail: hengke3@sina.com

References

[1] Ross GM. Induction of cell death by radiotherapy. Endocr Relat Cancer 1999; 6: 41-44.
[2] Bernier J, Hall EJ and Giaccia A. Radiation oncology: a century of achievements. Nat Rev Cancer 2004; 4: 737-747.
[3] Stone HB, Coleman CN, Anscher MS and McBride WH. Effects of radiation on normal tissue: consequences and mechanisms. Lancet Oncol 2003; 4: 529-536.
[4] Willey JS, Lloyd SA, Nelson GA and Bateman TA. Ionizing radiation and bone loss: space exploration and clinical therapy applications. Clin Rev Bone Miner Metab 2011; 9: 54-62.
[5] Suva LJ and Griffin RJ. The irradiation of bone: old idea, new insight. J Bone Miner Res 2012; 27: 747-748.
[6] Szymczyk KH, Shapiro IM and Adams CS. Ionizing radiation sensitizes bone cells to apoptosis. Bone 2004; 34: 148-156.
[7] Dudziak ME, Saadeh PB, Mehrara BJ, Steinbrech DS, Greenwald JA, Gittes GK and Longaker MT. The effects of ionizing radiation on osteoblast-like cells in vitro. Plast Reconstr Surg 2000; 106: 1049-1061.
[8] Baxter NN, Habermann EB, Tepper JE, Durham SB and Virnig BA. Risk of pelvic fractures in older women following pelvic irradiation. JAMA 2005; 294: 2587-2593.
[9] Igdem S, Alco G, Ercan T, Barlan M, Ganiyusufoglu K, Unalan B, Turkan S and Okkan S. Insufficiency fractures after pelvic radiotherapy in patients with prostate cancer. Int J Radiat Oncol Biol Phys 2010; 77: 818-823.
[10] Holt GE, Griffin AM, Pintilie M, Wunder JS, Catton C, O'Sullivan B and Bell RS. Fractures following radiotherapy and limb-salvage surgery for lower extremity soft-tissue sarcomas. A comparison of high-dose and low-dose radiotherapy. J Bone Joint Surg Am 2005; 87: 315-319.
[11] Meirow D and Nugent D. The effects of radiotherapy and chemotherapy on female reproduction. Hum Reprod Update 2001; 7: 535-543.
[12] Sparks RB, Crowe EA, Wong FC, Toohey RE and Siegel JA. Radiation dose distributions in normal tissue adjacent to tumors containing (131) I or (90)Y: the potential for toxicity. J Nucl Med 2002; 43: 1110-1114.
[13] Chargari C, Goodman KA, Diallo I, Guy JB, Rancoule C, Cosset JM, Deutsch E and Magne N. Risk of second cancers in the era of modern radiation therapy: does the risk/benefit analysis overcome theoretical models? Cancer Metastasis Rev 2016; 35: 277-288.
[14] Pierce SM, Recht A, Lingos TI, Abner A, Vicini F, Silver B, Herzog A and Harris JR. Long-term radiation complications following conservative surgery (CS) and radiation therapy (RT) in patients with early stage breast cancer. Int J Radiat Oncol Biol Phys 1992; 23: 915-923.
[15] Mitchell MJ and Logan PM. Radiation-induced changes in bone. Radiographics 1998; 18: 1125-1243.

[16] Williams HJ and Davies AM. The effect of X-rays on bone: a pictorial review. Eur Radiol 2006; 16: 619-633.
[17] Kwon JW, Huh SJ, Yoon YC, Choi SH, Jung JY, Oh D and Choe BK. Pelvic bone complications after radiation therapy of uterine cervical cancer: evaluation with MRI. AJR Am J Roentgenol 2008; 191: 987-994.
[18] Ikushima H, Osaki K, Furutani S, Yamashita K, Kishida Y, Kudoh T and Nishitani H. Pelvic bone complications following radiation therapy of gynecologic malignancies: clinical evaluation of radiation-induced pelvic insufficiency fractures. Gynecol Oncol 2006; 103: 1100-1104.
[19] Kristensen B, Ejlertsen B, Mouridsen HT, Andersen KW and Lauritzen JB. Femoral fractures in postmenopausal breast cancer patients treated with adjuvant tamoxifen. Breast Cancer Res Treat 1996; 39: 321-326.
[20] Chen Z, Maricic M, Aragaki AK, Mouton C, Arendell L, Lopez AM, Bassford T and Chlebowski RT. Fracture risk increases after diagnosis of breast or other cancers in postmenopausal women: results from the Women's Health Initiative. Osteoporos Int 2009; 20: 527-536.
[21] Willey JS, Livingston EW, Robbins ME, Bourland JD, Tirado-Lee L, Smith-Sielicki H and Bateman TA. Risedronate prevents early radiation-induced osteoporosis in mice at multiple skeletal locations. Bone 2010; 46: 101-111.
[22] Keenawinna L, Oest ME, Mann KA, Spadaro J and Damron TA. Zoledronic acid prevents loss of trabecular bone after focal irradiation in mice. Radiat Res 2013; 180: 89-99.
[23] Rachner TD, Khosla S and Hofbauer LC. Osteoporosis: now and the future. Lancet 2011; 377: 1276-1287.
[24] Massague J. Receptors for the TGF-beta family. Cell 1992; 69: 1067-1070.
[25] Baud'huin M, Solban N, Cornwall-Brady M, Sako D, Kawamoto Y, Liharska K, Lath D, Bouxsein ML, Underwood KW, Ucran J, Kumar R, Pobre E, Grinberg A, Seehra J, Canalis E, Pearsall RS and Croucher PI. A soluble bone morphogenetic protein type IA receptor increases bone mass and bone strength. Proc Natl Acad Sci U S A 2012; 109: 12207-12212.
[26] Keller S, Nickel J, Zhang JL, Sebald W and Mueller TD. Molecular recognition of BMP-2 and BMP receptor IA. Nat Struct Mol Biol 2004; 11: 481-488.
[27] Hatta T, Konishi H, Katoh E, Natsume T, Ueno N, Kobayashi Y and Yamazaki T. Identification of the ligand-binding site of the BMP type IA receptor for BMP-4. Biopolymers 2000; 55: 399-406.
[28] Wozney JM. The bone morphogenetic protein family and osteogenesis. Mol Reprod Dev 1992; 32: 160-167.
[29] Mishina Y, Starbuck MW, Gentile MA, Fukuda T, Kasparcova V, Seedor JG, Hanks MC, Amling M, Pinero GJ, Harada S and Behringer RR. Bone morphogenetic protein type IA receptor signaling regulates postnatal osteoblast function and bone remodeling. J Biol Chem 2004; 279: 27560-27566.
[30] Kamiya N, Ye L, Kobayashi T, Lucas DJ, Mochida Y, Yamauchi M, Kronenberg HM, Feng JQ and Mishina Y. Disruption of BMP signaling in osteoblasts through type IA receptor (BMPRIA) increases bone mass. J Bone Miner Res 2008; 23: 2007-2017.
[31] Kamiya N, Kobayashi T, Mochida Y, Yu PB, Yamauchi M, Kronenberg HM and Mishina Y. Wnt inhibitors Dkk1 and Sost are downstream targets of BMP signaling through the type IA receptor (BMPRIA) in osteoblasts. J Bone Miner Res 2010; 25: 200-210.
[32] Lim J, Shi Y, Karner CM, Lee SY, Lee WC, He G and Long F. Dual function of Bmpr1a signaling in restricting preosteoblast proliferation and stimulating osteoblast activity in mouse. Development 2016; 143: 339-347.
[33] Okamoto M, Murai J, Imai Y, Ikegami D, Kamiya N, Kato S, Mishina Y, Yoshikawa H and Tsumaki N. Conditional deletion of Bmpr1a in differentiated osteoclasts increases osteoblastic bone formation, increasing volume of remodeling bone in mice. J Bone Miner Res 2011; 26: 2511-2522.
[34] Kamiya N, Ye L, Kobayashi T, Mochida Y, Yamauchi M, Kronenberg HM, Feng JQ and Mishina Y. BMP signaling negatively regulates bone mass through sclerostin by inhibiting the canonical Wnt pathway. Development 2008; 135: 3801-3811.
[35] Ko FC, Van Vliet M, Ellman R, Grasso D, Brooks DJ, Spatz JM, Conlon C, Aguirre JI, Wronski TJ and Bouxsein ML. Treatment with a soluble bone morphogenetic protein type 1A receptor (BMPR1A) fusion protein increases bone mass and bone formation in mice subjected to hindlimb unloading. JBMR Plus 2017; 1: 66-72.
[36] Wright LE, Buijs JT, Kim HS, Coats LE, Scheidler AM, John SK, She Y, Murthy S, Ma N, Chin-Sinex HJ, Bellido TM, Bateman TA, Mendonca MS, Mohammad KS and Guise TA. Single-limb irradiation induces local and systemic bone loss in a murine model. J Bone Miner Res 2015; 30: 1268-1279.
[37] Zhang J, Zheng L, Wang Z, Pei H, Hu W, Nie J, Shang P, Li B, Hei TK and Zhou G. Lowering iron level protects against bone loss in focally irradiated and contralateral femurs through distinct mechanisms. Bone 2019; 120: 50-60.
[38] Miao D, Su H, He B, Gao J, Xia Q, Zhu M, Gu Z, Goltzman D and Karaplis AC. Severe growth retardation and early lethality in mice lacking the

nuclear localization sequence and C-terminus of PTH-related protein. Proc Natl Acad Sci U S A 2008; 105: 20309-20314.
[39] Parfitt AM, Drezner MK, Glorieux FH, Kanis JA, Malluche H, Meunier PJ, Ott SM and Recker RR. Bone histomorphometry: standardization of nomenclature, symbols, and units. Report of the ASBMR Histomorphometry Nomenclature Committee. J Bone Miner Res 1987; 2: 595-610.
[40] Jing D, Luo E, Cai J, Tong S, Zhai M, Shen G, Wang X and Luo Z. Mechanical vibration mitigates the decrease of bone quantity and bone quality of leptin receptor-deficient Db/Db mice by promoting bone formation and inhibiting bone resorption. J Bone Miner Res 2016; 31: 1713-1724.
[41] Miao DS, Bai XY, Panda D, McKee MD, Karaplis AC and Goltzman D. Osteomalacia in Hyp mice is associated with abnormal Phex expression and with altered bone matrix protein expression and deposition. Endocrinology 2001; 142: 926-939.
[42] Geng Q, Gao H, Yang R, Guo K and Miao D. Pyrroloquinoline quinone prevents estrogen deficiency-induced osteoporosis by inhibiting oxidative stress and osteocyte senescence. Int J Biol Sci 2019; 15: 58-68.
[43] Dempster DW, Compston JE, Drezner MK, Glorieux FH, Kanis JA, Malluche H, Meunier PJ, Ott SM, Recker RR and Parfitt AM. Standardized nomenclature, symbols, and units for bone histomorphometry: a 2012 update of the report of the ASBMR Histomorphometry Nomenclature Committee. J Bone Miner Res 2013; 28: 2-17.
[44] Xue Y, Zhang Z, Karaplis AC, Hendy GN, Goltzman D and Miao D. Exogenous PTH-related protein and PTH improve mineral and skeletal status in 25-hydroxyvitamin D-1alpha-hydroxylase and PTH double knockout mice. J Bone Miner Res 2005; 20: 1766-1777.
[45] Jackson A, Vayssiere B, Garcia T, Newell W, Baron R, Roman-Roman S and Rawadi G. Gene array analysis of Wnt-regulated genes in C3H10T1/2 cells. Bone 2005; 36: 585-598.
[46] Chandra A, Lin T, Young T, Tong W, Ma X, Tseng WJ, Kramer I, Kneissel M, Levine MA, Zhang Y, Cengel K, Liu XS and Qin L. Suppression of sclerostin alleviates radiation-induced bone loss by protecting bone-forming cells and their progenitors through distinct mechanisms. J Bone Miner Res 2017; 32: 360-372.
[47] Zenger S, Hollberg K, Ljusberg J, Norgard M, Ek-Rylander B, Kiviranta R and Andersson G. Proteolytic processing and polarized secretion of tartrate-resistant acid phosphatase is altered in a subpopulation of metaphyseal osteoclasts in cathepsin K-deficient mice. Bone 2007; 41: 820-832.
[48] Fuller K, Lawrence KM, Ross JL, Grabowska UB, Shiroo M, Samuelsson B and Chambers TJ. Cathepsin K inhibitors prevent matrix-derived growth factor degradation by human osteoclasts. Bone 2008; 42: 200-211.
[49] Takayanagi H, Kim S, Koga T, Nishina H, Isshiki M, Yoshida H, Saiura A, Isobe M, Yokochi T, Inoue J, Wagner EF, Mak TW, Kodama T and Taniguchi T. Induction and activation of the transcription factor NFATc1 (NFAT2) integrate RANKL signaling in terminal differentiation of osteoclasts. Dev Cell 2002; 3: 889-901.
[50] Lee SH, Rho J, Jeong D, Sul JY, Kim T, Kim N, Kang JS, Miyamoto T, Suda T, Lee SK, Pignolo RJ, Koczon-Jaremko B, Lorenzo J and Choi Y. v-ATPase V0 subunit d2-deficient mice exhibit impaired osteoclast fusion and increased bone formation. Nat Med 2006; 12: 1403-1409.
[51] Zaidi M. Skeletal remodeling in health and disease. Nat Med 2007; 13: 791-801.
[52] Glass DA, 2nd, Bialek P, Ahn JD, Starbuck M, Patel MS, Clevers H, Taketo MM, Long F, McMahon AP, Lang RA and Karsenty G. Canonical Wnt signaling in differentiated osteoblasts controls osteoclast differentiation. Dev Cell 2005; 8: 751-764.
[53] Manolagas SC. Wnt signaling and osteoporosis. Maturitas 2014; 78: 233-237.
[54] Bonewald LF and Johnson ML. Osteocytes, mechanosensing and Wnt signaling. Bone 2008; 42: 606-615.
[55] Kramer I, Halleux C, Keller H, Pegurri M, Gooi JH, Weber PB, Feng JQ, Bonewald LF and Kneissel M. Osteocyte Wnt/beta-catenin signaling is required for normal bone homeostasis. Mol Cell Biol 2010; 30: 3071-3085.
[56] Takebe N, Miele L, Harris PJ, Jeong W, Bando H, Kahn M, Yang SX and Ivy SP. Targeting Notch, Hedgehog, and Wnt pathways in cancer stem cells: clinical update. Nat Rev Clin Oncol 2015; 12: 445-464.